

## Midinfrared photoconductivity of Ge/Si self-assembled quantum dots

N. Rappaport and E. Finkman

*Department of Electrical Engineering and Solid State Institute, Technion, Haifa 32000, Israel*

T. Brunhes, P. Boucaud,<sup>a)</sup> S. Sauvage, N. Yam, V. Le Thanh, and D. Bouchier

*Institut d'Électronique Fondamentale, UMR CNRS 8622, Bâtiment 220, Université Paris-Sud, 91405 Orsay, France*

(Received 10 July 2000; accepted for publication 8 September 2000)

We have investigated the midinfrared photoconductivity of Ge/Si self-assembled quantum dots. The self-assembled quantum dots were grown by ultra-high-vacuum chemical vapor deposition on Si(001). The photoresponse of the *p*-type device exhibits resonances in the midinfrared around 10  $\mu\text{m}$  wavelength. The resonance of the photocurrent shifts to lower energy as the applied bias increases. The photocurrent is weakly dependent on the incoming polarization of the infrared light. The photocurrent is analyzed in terms of bound-to-bound and bound-to-continuum transitions in the valence band. The photocurrent peaks are correlated to the photoluminescence of the device.  
© 2000 American Institute of Physics. [S0003-6951(00)04046-8]

Quantum dot infrared photodetectors have been the subject of extensive studies in recent years. The operation principle of quantum dot photodetectors is similar to that of quantum well intersubband photodetectors.<sup>1</sup> The detector is a photoconductor with an active region which consists of doped semiconductor quantum dots. Under infrared excitation carriers are photoexcited via intraband absorption and give rise to a photocurrent. One advantage of using quantum dots instead of quantum wells relies on an expected larger photoconductive gain associated with a reduced capture probability. Another advantage is related to the nonvanishing normal incidence absorption which can be observed in quantum dots.<sup>2–4</sup> Several groups have recently reported on the growth and on the characterization of infrared photodetectors using self-assembled quantum dots.<sup>5–8</sup>

Most of the demonstrations of quantum dot photodetectors were achieved with III–V heterostructures. Si-based quantum dot infrared photodetectors represent another attractive type of device. The main advantage of Si-based photodetectors is its compatibility with complementary metal-oxide-semiconductor (CMOS) readout circuitry. This compatibility could lead to the monolithic integration of photodetectors with Si-based electronics. The integration on Si is expected to avoid such problems encountered for large-area infrared focal plane arrays like the thermal mismatch between III–V and IV–IV materials. Si-based self-assembled quantum dots can be easily obtained using the Stranski–Krastanow growth mode between lattice-mismatched Ge and Si.<sup>9–11</sup> The 4.2% lattice mismatch between Ge and Si leads usually to the formation of islands with a small aspect ratio (height/base width). A significant valence band offset exists between both strained and relaxed Ge on Si. The existence of this valence band offset has led, in recent years, to the realization of *p*-type devices like Si-based valence band intersubband photodetectors using SiGe quantum wells.<sup>12–14</sup> Midinfrared in-plane polarized and *z*-polarized intraband absorption has been recently evidenced in the valence band of

Ge/Si self-assembled quantum dots.<sup>15,16</sup> These measurements have opened the route to the realization of Si-based quantum dot infrared photodetectors. First measurements of midinfrared photoconductivity have been reported for Ge/Si quantum dots grown by molecular beam epitaxy.<sup>17,18</sup>

The self-assembled quantum dots were grown on Si(001) substrates by ultra-high-vacuum chemical vapor deposition using silane and germane as gas precursors. The growth temperature was 600 °C and the gas pressure around  $5 \times 10^{-4}$  Torr during epitaxial growth. The active region consists of 10 Ge quantum dot layers separated by 31 nm thick Si barriers. The active region was embedded between two *p*<sup>+</sup> doped Si layers to provide ohmic contacts. A 1 nm thick *p*-type modulation doping with boron ( $5 \times 10^{16} \text{ cm}^{-3}$ ) was inserted 1 nm below the Ge dots in sample A206. This modulation doping is expected to provide an average concentration of about two carriers per dot. The active region of one reference sample (A203) was not intentionally doped. From atomic force microscopy and cross section transmission electron microscopy images, the dot density is estimated to be  $1–2 \times 10^9 \text{ cm}^{-2}$ . The mean dot base length is 100 nm and the average dot height is around 5–7 nm. The dot uniformity is  $\pm 10\%$ . In a previous publication,<sup>19</sup> we have shown that the onset of the two- to three-dimensional growth mode transition is modified by the vertical stacking of multiple quantum dot layers. The critical thickness corresponding to the onset of the dot nucleation decreases from one layer to another because of the strain field. In order to account for this effect, the thickness of the deposited Ge was decreased from the first layer to the last layer. This feature leads to a better vertical homogeneity of the quantum dots.

Photodetector  $200 \mu\text{m} \times 200 \mu\text{m}$  mesas were processed by standard photolithography and by wet chemical etching up to the Si bottom contact. Al ohmic contacts were evaporated and alloyed on the top and bottom contact layers. The samples were polished with 45° wedge after processing to test the polarization dependence of the photocurrent. The photoresponse was measured with a Fourier transform infrared spectrometer.

<sup>a)</sup>Electronic mail: phill@ief.u-psud.fr

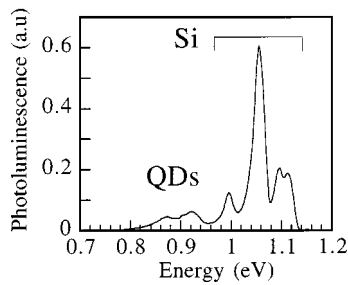


FIG. 1. Low-temperature (2.8 K) photoluminescence spectrum of sample A203. The quantum dot recombination is observed on the low energy side of the spectrum. The photoluminescence was excited with an argon ion laser (200 mW focused on a 5 mm diameter spot).

The low temperature photoluminescence spectrum of the reference sample (A203) is shown in Fig. 1. The photoluminescence is dominated by the transverse-optical phonon-assisted recombination in the doped Si layers at 1056 meV.<sup>20</sup> The corresponding no-phonon recombination is observed at 1113 meV. The phonon-assisted bound-exciton recombination occurring in the Si barrier layers is observed at 1094 meV. The resonance at 997 meV is attributed to a recombination in the doped Si layers involving a TO phonon and one optical zone-center phonon  $O^T$ . The quantum dot recombination is observed at lower energy. The emission of the self-assembled quantum dots exhibits a maximum of 925 meV along with a weaker emission at lower energy around 875 meV.

Figure 2 shows the current–voltage characteristic of sample A206 as a function of the temperature. The curve marked by dots represents the photocurrent measured with an aperture  $f/1$  at 17 K in the presence of a 300 K background. The shape of the current is asymmetric versus the applied bias. A kink is observed at negative bias around  $-1$  V. The asymmetry in the photocurrent is likely attributed to the asymmetry introduced by the doping of the sample and by the asymmetry of the quantum dots.<sup>21</sup>

The spectral dependence of the photocurrent of the  $p$ -type device (A206) is shown in Fig. 3. The photocurrent was measured as a function of the applied bias for a sample temperature of 18 K. Figure 3(a) corresponds to an  $s$ -polarized excitation (polarization in the layer plane of the dots). Figure 3(b) corresponds to a  $p$ -polarized excitation (50% of the electric field in the layer plane and 50% of the electric field along the growth axis of the dots). The photocurrent is maximum around 10  $\mu\text{m}$  wavelength. The amplitude of the integrated photocurrent is similar for  $p$  and  $s$

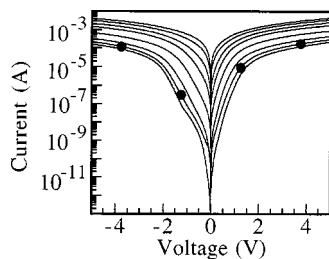


FIG. 2. Current–voltage characteristic of sample A206 as a function of the temperature. From bottom to top: 15, 26, 40, 50, 60, 70, and 80 K. The curve marked by dots shows the photocurrent measured at 17 K with a 300 K background and with an aperture  $f/1$ .

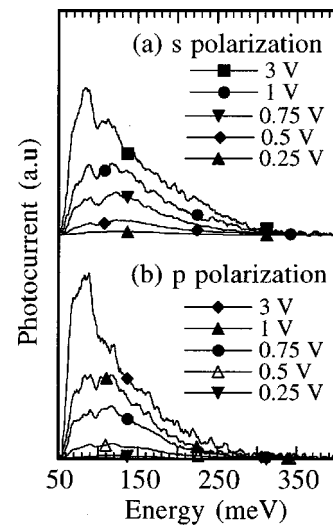


FIG. 3. (a) Photoresponse of sample A206 as a function of the applied bias in  $s$ -polarization [(b)  $p$  polarization]. The sample temperature is 18 K. The curves have been offset for clarity. The applied biases are indicated in the insets.

polarizations. This result demonstrates the ability of these photodetectors to operate at normal incidence. Similar photocurrent spectra were obtained for a normal-incidence illumination. The photocurrent exhibits several resonances as a function of the applied bias. At low applied bias, the resonances at 120 and 160 meV are dominant. As the applied bias increases, the 160 meV resonance is quenched. Meanwhile, the amplitude of the photocurrent at low energy (90 meV) increases. At high applied bias, the photocurrent is dominated by the 90 meV resonance. A similar behavior is observed for negative applied biases. The photoresponse first exhibits a linear dependence on the applied bias at low voltage, then a superlinear dependence up to 1 V and a sublinear dependence at higher voltage. We attribute the sublinear dependence of the photoresponse at high voltage to a depletion of the quantum dot layers.

We now discuss the origin of the different photocurrent resonances. Figure 4 shows the photocurrent response of the device in  $p$  polarization for a 0.11 V applied bias. The photocurrent measured in  $s$  polarization is also shown for comparison. It is worth noting that, at high energy, the photocurrent is larger in  $p$  than  $s$  polarization, thus indicating the contribution of  $z$ -polarized transitions to the photocurrent. The resonances at 120 and 160 meV are clearly observed. A weak shoulder is also observed at 90 meV. This feature will

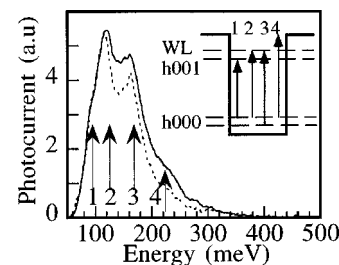


FIG. 4. Photoresponse of sample A206 in  $p$  polarization for a 0.11 V applied bias. The dashed line corresponds to the photocurrent measured in  $s$  polarization. The sample temperature is 20 K. The inset shows a schematic diagram of the different intraband transitions involved in the photoconductivity.

become the dominant contribution at high applied bias. A small resonance is observed at higher energy around 230 meV. In a previous work, we did report on the midinfrared photoinduced absorption in Ge/Si self-assembled quantum dots.<sup>16</sup> An in-plane polarized resonant absorption around 290 meV was observed for samples exhibiting a photoluminescence resonance at 865 meV. The energy of this transition was close to the energy difference between the Si band gap and the no-phonon photoluminescence of the self-assembled quantum dots. This absorption was therefore attributed to a bound-to-continuum transition between the ground state of the quantum dots and the continuum states lying above the quantum dots. In the case of sample A206, the photoluminescence is peaked at 925 meV. The bound-to-continuum transition is therefore expected to be maximum around 225 meV. Consequently, we attribute the weak resonance of the photocurrent around 230 meV to the intraband transitions between the dot ground states to the continuum states in the silicon barriers. In Ref. 22, the composition of the Ge/Si self-assembled dots was estimated by selected-area electronic diffraction pattern of a single dot to be around 50%. Because of the flat shape of the dots, the energy of the intersublevel transition from the ground state ( $h_{000}$ ) to the first confined state along the  $z$ -growth axis ( $h_{001}$ ) can be estimated at first order by the heavy-hole intersubband energy  $HH_0-HH_1$  of a 6 nm thick  $Si_{0.5}Ge_{0.5}$  quantum well. By neglecting band mixing with light hole and spin-orbit splitoff bands, the intersubband energy is calculated at 95 meV. We attribute the origin of the 90 meV resonance which dominates the photocurrent spectrum at high applied bias to the bound-to-bound transition between the confined states in the quantum dots ( $h_{000}-h_{001}$ ). One would expect this transition to be  $z$  polarized. The lack of polarization dependence is a signature of the strong band-mixing effects in the valence band of these alloyed layers. The sharp increase of the 90 meV photocurrent response with the applied bias is consistent with a bound-to-bound origin. At high applied bias, the photoexcited carriers are more likely to tunnel out of the dots and generate a strong photocurrent. The origin of the 120 and 160 meV resonances is more ambiguous. We do not observe the photoluminescence associated with the wetting layers in these photodetector samples. In Ref. 19, the no-phonon photoluminescence of the wetting layers was observed around 1030 meV. The intraband transition from the dot ground state to the two-dimensional wetting layer state is therefore expected to be around 105 meV. We note that the vertical stacking of quantum dot layers is likely to introduce inhomogeneities from layer to layer. Part of the photoluminescence resonance observed at 875 meV could originate from a no-phonon recombination of quantum dots with a different composition or size, and not from a phonon-assisted recombination. In that case, the intraband transition from the ground state to the wetting layer states would occur at 155 meV. Based on the preceding arguments, we tentatively assign the resonances at 120 and 160 meV to intraband transitions from

the dot ground states to the wetting layer states. These resonances which dominate the photocurrent at low applied bias correspond to bound-to-continuum transitions. The origin of the different photocurrent resonances is summarized in the inset of Fig. 4. We emphasize that the photoresponse depends both on the absorption and on the vertical transport properties in the sample. In the case of SiGe quantum well intersubband detectors, the amplitude of the photocurrent was strongly different from the amplitude of the absorption.<sup>14</sup> This feature was explained by an energy-dependent photoconductive gain. A similar situation is likely to occur in the quantum dot photodetectors. The mixing between heavy holes, light holes and spin-orbit splitoff bands along with a more realistic dot confinement potential should also be considered for a detailed analysis of the photocurrent.

This work was supported by Association Franco-Israélienne pour la Recherche Scientifique et Technique (AFIRST).

<sup>1</sup>B. F. Levine, *J. Appl. Phys.* **74**, R1 (1993).

<sup>2</sup>H. Drexler, D. Leonard, W. Hansen, J. P. Kotthaus, and P. M. Petroff, *Phys. Rev. Lett.* **73**, 2252 (1994).

<sup>3</sup>S. Sauvage, P. Boucaud, J.-M. Gérard, and V. Thierry-Mieg, *Phys. Rev. B* **58**, 10562 (1998).

<sup>4</sup>We emphasize that grating couplers or random scatterers have been successfully developed for focal plane arrays based on intersubband quantum well photodetectors. A light coupling efficiency as high as 80% can be achieved for intersubband transitions polarized along the  $z$ -growth axis.

<sup>5</sup>J. Phillips, K. Kamath, and P. Bhattacharya, *Appl. Phys. Lett.* **72**, 2020 (1998).

<sup>6</sup>S. Maimon, E. Finkman, G. Bahir, S. E. Schacham, J. M. Garcia, and P. M. Petroff, *Appl. Phys. Lett.* **73**, 2003 (1998).

<sup>7</sup>D. Pan, E. Towe, and S. Kennerly, *Appl. Phys. Lett.* **73**, 1937 (1998).

<sup>8</sup>S. Kim, H. Mohseni, M. Erdtmann, E. Michel, C. Jelen, and M. Razeghi, *Appl. Phys. Lett.* **73**, 963 (1998).

<sup>9</sup>D. E. Eaglesham and M. Cerullo, *Phys. Rev. Lett.* **64**, 1943 (1990).

<sup>10</sup>P. Schittenhelm, M. Gail, J. Brunner, J. F. Nützel, and G. Abstreiter, *Appl. Phys. Lett.* **67**, 1292 (1995).

<sup>11</sup>V. Le Thanh, P. Boucaud, D. Débarre, Y. Zheng, D. Bouchier, and J.-M. Lourtioz, *Phys. Rev. B* **58**, 13115 (1998).

<sup>12</sup>J. S. Park, R. P. G. Karunasiri, and K. L. Wang, *Appl. Phys. Lett.* **61**, 681 (1992).

<sup>13</sup>R. People, J. C. Bean, S. K. Sputz, C. G. Bethea, and L. J. Peticolas, *Thin Solid Films* **222**, 120 (1992).

<sup>14</sup>P. Kruck, M. Helm, T. Fromherz, G. Bauer, J. F. Nützel, and G. Abstreiter, *Appl. Phys. Lett.* **69**, 3372 (1996).

<sup>15</sup>J. L. Liu, W. G. Wu, A. Ballandin, G. L. Jin, and K. L. Wang, *Appl. Phys. Lett.* **74**, 185 (1999).

<sup>16</sup>P. Boucaud, V. Le Thanh, S. Sauvage, D. Debarre, and D. Bouchier, *Appl. Phys. Lett.* **74**, 401 (1999).

<sup>17</sup>L. P. Rokhinson, D. C. Tsui, J. L. Benton, and Y.-H. Xie, *Appl. Phys. Lett.* **75**, 2413 (1999).

<sup>18</sup>C. Miesner, O. Röthig, K. Brunner, and G. Abstreiter, *Appl. Phys. Lett.* **76**, 1027 (2000).

<sup>19</sup>V. Le Thanh, V. Yam, P. Boucaud, F. Fortuna, C. Ulysse, D. Bouchier, L. Vervoort, and J.-M. Lourtioz, *Phys. Rev. B* **60**, 5851 (1999).

<sup>20</sup>J. Wagner, *Phys. Rev. B* **29**, 2002 (1984).

<sup>21</sup>H. C. Liu, A. G. Steele, M. Buchanan, and Z. R. Wasilewski, *J. Appl. Phys.* **73**, 2029 (1993).

<sup>22</sup>G. Patriarche, I. Sagnes, P. Boucaud, V. Le Thanh, D. Bouchier, C. Hernandez, Y. Campidelli, O. Kernmarrec, and D. Bensahel, *Appl. Phys. Lett.* **77**, 370 (2000).